Journal of
Materials Chemistry C

Structural Effects on the Charge Transport Properties of Chemically and Electrochemically Doped Dioxythiophene Polymers

Journal:	*Journal of Materials Chemistry C*
Manuscript ID	TC-ART-10-2019-005697.R1
Article Type:	Paper
Date Submitted by the Author:	16-Nov-2019
Complete List of Authors:	Reynolds, John; Georgia Institute of Technology, Chemistryand Biochemistry, Materials Science and Engineering Pittelli, Sandra; Georgia Institute of Technology, Chemistry and Biochemistry De Keersmaecker, Michel; Georgia Institute of Technology, Chemistryand Biochemistry Ponder, James; Georgia Institute of Technology Ochieng, Melony; Georgia Institute of Technology, Chemistryand Biochemistry Österholm, Anna; Georgia Institute of Technology,

Structural Effects on the Charge Transport Properties of Chemically and Electrochemically Doped Dioxythiophene Polymers

Sandra L. Pittelli, Michel De Keersmaeker, James F. Ponder Jr.,‡ Anna M. Österholm, Melony A. Ochieng, and John R. Reynolds*

School of Chemistry and Biochemistry, School of Materials Science and Engineering, Center for Organic Photonics and Electronics, Georgia Tech Polymer Network, Georgia Institute of Technology, Atlanta, GA, USA.

E-mail: reynolds@chemistry.gatech.edu

‡ *Present address: Department of Chemistry, Imperial College London, London, United Kingdom.*

Keywords: Dioxythiophenes, Redox Doping, Conductive Polymers, Chemical Doping, Ion Transport, Mixed Conductors

Abstract:

We evaluate a set of two 3,4-propylenedioxythiophene (ProDOT) and two acyclic dioxythiophene (AcDOT) homopolymers with each type of XDOT having either branched or linear solubilizing side chains. We show that while altering the structure of the polymer does have an effect on the degree of intermolecular ordering of the polymer film, these as-cast morphologies are not correlated with enhanced charge transport properties. When using linear n-octyl solubilizing side chains rather than branched ethylhexyl chains, we see a multiple order of magnitude increase in the solid-state electrical conductivity for both ProDOT and AcDOT polymers. When using an ammoniumyl-based dopant (Magic Blue) as a chemical oxidant, these polymers show conductivities on the order of 10^0 S/cm. In terms of redox properties, linear side chains lower the onset of oxidation by 300 mV and increase in the electrochemical conductance. Finally, the polymers substituted with linear side chains have higher ionic mobility implying that these more effective at transporting both electronic charge carriers and ions through the film.

Introduction:

A myriad of applications for conjugated polymers (CPs) have been explored due to their ability to simultaneously transport both ions and electrons. In general, CPs are desirable for both solid-state and redox applications because of their ability to reversibly transition between a charge neutral (insulating) and a charged (conducting) state through either chemical[1-8] or electrochemical oxidation.[9-11] Neutral CPs can undergo hole and electron injection, making them useful in solid-state applications including organic field effect transistors,[12] organic photovoltaics,[13] and thermoelectric generators.[14,15] In addition, CPs that have been chemically doped to a highly conducting state have been evaluated as e.g. transparent conductive electrodes.[16,17] CPs can also be redox-doped through electrochemical oxidation and used in applications such as electrochromic devices,[18-21] supercapacitors,[22-24] actuators,[25-28] organic electrochemical transistors,[29] and sensors[30,31] that all rely on efficient transport of both ions and electrons for optimal device operation. Regardless of the method of doping, charge balancing dopant anions and solvent molecules need to penetrate through the bulk of the film, and the polymer backbone needs to be able to undergo a planarization attributed to the formation of a quinoidal structure.

Significant effort has been put into understanding the structure-property relationships of these materials, mainly focusing on how the repeat unit structure affects both its electronic and ionic charge transport properties. Effort has also been made to induce solubility in CPs making them compatible with high-throughput printing and coating methods,[32] which typically involves incorporating long hydrocarbon or oligo(ethylene oxide) side chains onto the polymer backbone. Previous work established that manipulation of the polymer backbone affects solid-state charge transport properties

such as mobility,[33] and conductivity[34] and that these properties are greatly affected by the conformation,[35] degree of ordering and orientation of the polymer chains, which all depend on both the repeat unit structure, polymer solubility, and the processing method.[36-38] In terms of redox properties, the choice of repeat unit influences the charge capacity,[39] the onset of oxidation, and the redox kinetics.[40] Additionally, it has been shown that the structure of the solubilizing side chain also has an effect on the charge transport in both solid-state[32,41-44] and the redox properties.[45,46] Given the multitude of applications available for these materials, it is important to understand how structural modification affects both the semiconducting and redox properties of CPs. Studies have shown that higher degrees of intermolecular ordering can lead to enhanced electron transport, however, there is still a question as to how this affects ion transport with some examples suggesting that highly ordered materials inhibit the latter.[47,48]

Dioxythiophene (XDOT)-based materials are excellent candidates for use in solution-processed electrochemical devices.[18,49] Previous work has shown that a copolymer combining 3,4-propylenedioxythiophene (ProDOT) and 3,4-ethylenedioxythiophene (EDOT) units demonstrates high solid-state conductivity in the excess of 200 S cm^{-1} after chemical doping with $AgPF_6$.[50] Another recent study on oligoether functionalized poly(ProDOT) achieved solid-state conductivities of ~ 1 S cm^{-1} after doping with the chemical oxidant, 2,3,5,6-tetrafluoro-tetracyanoquinodimethane (F4TCNQ).[51]

In this work, we gain a comprehensive understanding of how manipulation of the structure of both the conjugated polymer backbone and the solubilizing side chain affect the morphology, and how this alteration in morphology affects the material's ionic and electronic charge transport properties. To achieve this, we evaluate a set of two 3,4-

propylenedioxythiophene (ProDOT) and two acyclic dioxythiophene (AcDOT) homopolymers with each type of XDOT having either branched or linear alkyl solubilizing side chains. This family of polymers focuses on materials that have a di-substituted thiophene ring, which protects the polymer backbone from nucleophilic attack and ensures reversible and stable redox doping. The ProDOT and AcDOT moieties differ in their presence or lack of a propylene bridge substituted onto the dioxythiophene ring. This bridge causes two primary steric effects: (1) increasing the distance between the solubilizing side chain and the polymer backbone and (2) positioning these side chains out of plane relative to the backbone direction. Furthermore, this bridge changes the ability of the lone pair of electrons on the oxygen atoms to interact with the conjugated π-system of the thiophene ring, adding to the electron richness of the backbone allowing us to probe both steric and electronic effects. Comparisons of branched and linear alkyl side chains in benzodithiophene-based co-polymers show evidence of changes in charge transport, aggregation, and degree of ordering depending on the choice of side chain.[45] To be able to clearly elucidate the steric effects from the side chains, we compare homopolymers where every thiophene ring is substituted with a solubilizing group. We show that changing the side chain from a branched to a linear n-alkyl structure makes the polymer easier to oxidize, and increases the electrical solid-state conductivity, electrochemical conductance, and ionic conductivity.

Results:

Approach

For this study, we designed and synthesized a family of four homopolymers based on ProDOTs (Pro) and AcDOTs (Ac), that contain either ethylhexyl (Pro-EH and Ac-EH)

or linear n-octyl (Pro-Oct and Ac-Oct) aliphatic side chains, and substitution of these side chains at varying distances from, and orientations to, the conjugated core as depicted in Scheme 1. Details on the synthesis, purity, and molecular weights of the materials can be found in Figures S1-S6.

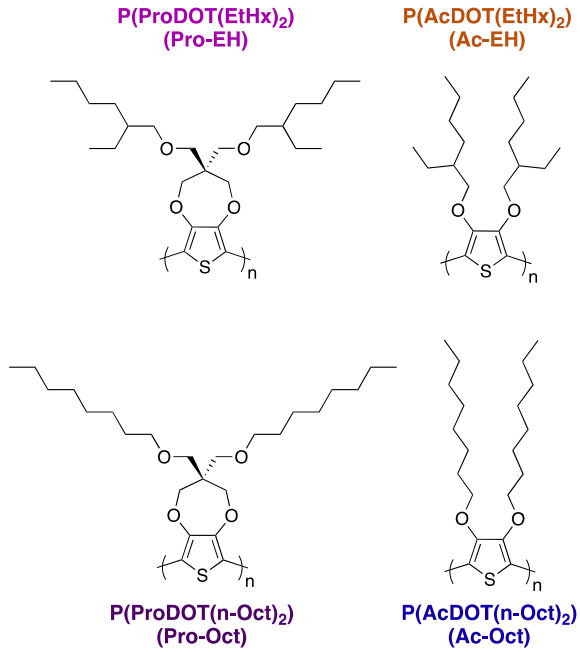

Scheme 1: Repeat unit structures of the family of the polymers used in this study.

The top two polymers in Scheme 1, Pro-EH and Ac-EH, have been previously shown to be colored-to-colorless electrochromic materials,[52,53] however the ProDOT analogue demonstrated much faster doping kinetics and more effective bleaching of the neutral state absorption peak than the Ac counterpart. The bottom two, Pro-Oct and Ac-Oct, were specifically synthesized for this work in order to compare the effects of using linear or branched solubilizing aliphatic side chains to probe how this would enhance or hinder the degree of intermolecular ordering, solid-state conductivity, onset of oxidation, charge capacity, and doping kinetics of the CPs.

Polymer Film Morphology

Intermolecular ordering and surface topography have been shown to have a large influence on the overall charge transport properties of CPs.[34-38] Two methods for evaluating these properties are Grazing-Incidence Wide-Angle X-ray Scattering (GIWAXS) and Atomic Force Microscopy (AFM). GIWAXS experiments provide information about the degree of intermolecular ordering of polymer chains, whereas AFM can provide information regarding the surface topology and the film roughness. Both measurements can provide insight as to why charge transport may be enhanced or inhibited for a given polymer as a result of the as-cast morphology or a change in the morphology after doping. Studies conducted on poly(3-hexylthiophene) (P3HT) for example, show that chemical oxidation gives rise to solid-state conductivities up to 8 S cm^{-1},[1] but that a prerequisite for efficient doping and high conductivity is a delicate balance between the degree of aggregation and intermolecular ordering in the film.[54] For the non-aggregating oligoether functionalized poly(ProDOT), it was shown that there was no crystalline ordering in samples that had been solution doped prior to casting whereas vapor doped samples did exhibit crystalline ordering as well as significant texturing relative to the substrate. In this case however, the degree of order did not influence the magnitude of electrical conductivity.[51]

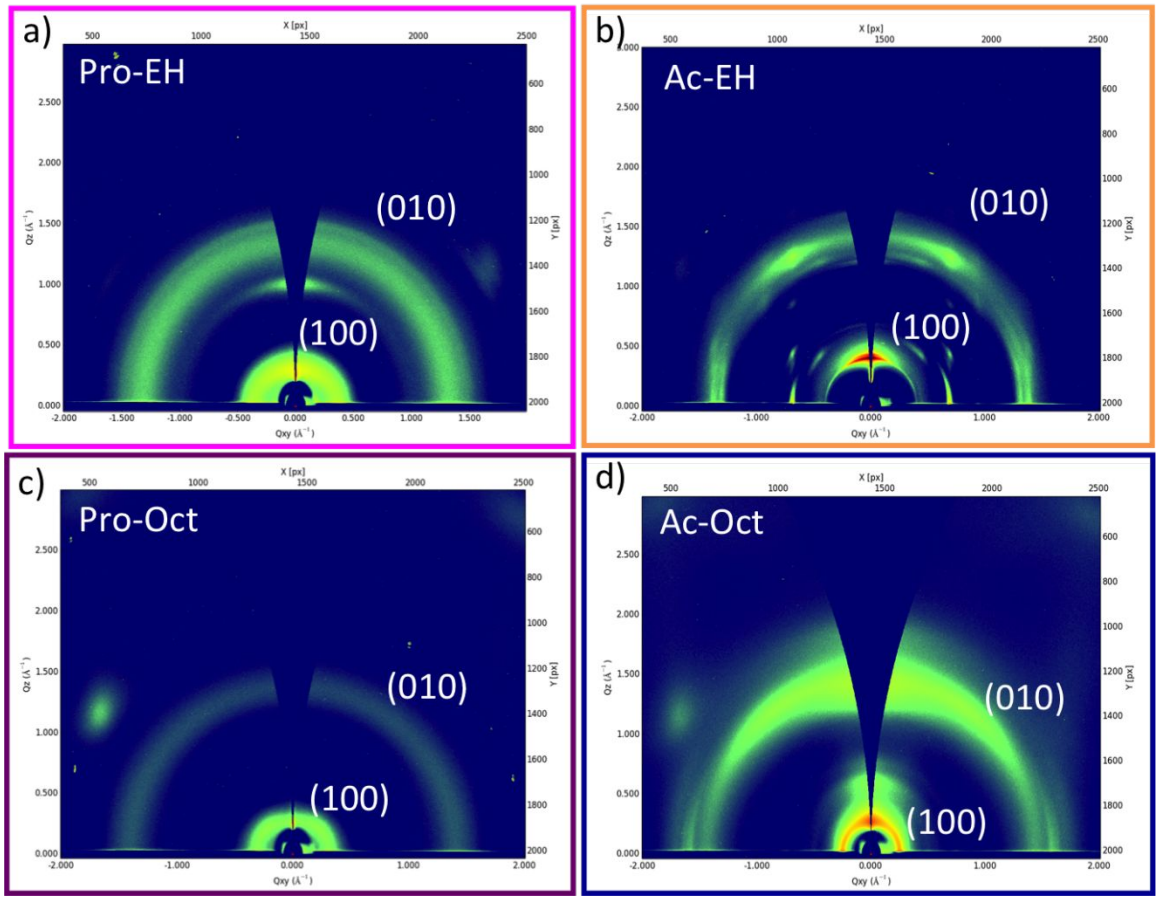

Fig. 1: GIWAXS images of as-cast, blade-coated films of (a) Pro-EH, (b) Ac-EH, (c) Pro-Oct, (d) Ac-Oct.

To probe potential differences in the polymers studied here, GIWAXS measurements were performed on blade-coated films, where the data corresponding to the polymers with branched side chains is shown in Fig. 1a and 1b, and the data corresponding to the linear analogues is shown in Fig. 1c and 1d. The 2D detector images reveal that the chosen backbone repeat unit has a large impact on the preferential scattering direction. The Pro polymers (Fig. 1a and 1c) are isotropic materials as evidenced by the large halos in both the (100) and the (010) planes, indicating that the polymer chains have no preferential ordering in terms of directionality relative to the substrate. In contrast, the GIWAXS

images of the Ac polymers (Fig. 1b and 1d) exhibit more ordered domains, as evidenced by the high intensity small area signals (for Ac-EH) and the preferential in-plane orientation for Ac-Oct, shown by the narrower lamellar scattering (100) along the Q_{xy} axis and π-π (010) scattering peaks along the Q_z axis. Further evaluation was done based on the overlay of the linecuts along the Q_z direction in Fig. S7a showing important information about the short-range intermolecular ordering. For Pro-EH, Pro-Oct, and Ac-Oct the diffraction band is seen at $Q_z \approx 0.27$ Å^{-1} (interplanar distance d ≈ 23 Å). For the Ac-EH polymer, a shift is observed towards tighter lamellar packing (d ≈ 15.8 Å), which is explained by combination of the lack of the propylene bridge on the thiophene ring and the steric bulk of the branched ethylhexyl side chains. In the case of the π-π distances, all polymers are in the same range (d ≈ 4.5 Å). For comparison, the work done by Mazaheripour et al. shows that a ProDOT polymer with oligoether side chains (9 atoms) has a lamellar spacing of 25.8 Å and π-π spacing of 3.5 Å.[51] Here, we observe tighter lamellar packing by 2 Å, which can be explained by the shorter side chains used in our work (8 atoms), and significantly larger π-π spacing distance (~4.5 Å). In the AFM height images (Fig. S8) we see that the Ac polymers form smoother films than the Pro polymers. In the phase images (Fig. S9) the darker regions are indicative of softer film domains and then bright regions are indicative of stiffer domains. Both Ac polymers have distinct phases showing fibril-like structures, which correlates well with the higher degrees of ordering demonstrated by their corresponding diffraction images. In contrast, the AFM images of the Pro polymers show no distinct phases, which correlate well with the GIWAXS images showing more isotropic distributions.

Chemical and Electrochemical Doping

In general, pre-cast neutral CP films are oxidized in two ways: through chemical oxidation by reaction with an electron-accepting molecule, or through electrochemical oxidation (preferably in a three-electrode cell where the working electrode potential can be controlled). Both routes involve the incorporation of charge-balancing dopant anions and solvent molecules resulting in polymer swelling, as well as the planarization of the polymer backbone attributed to the formation of a quinoid structure, which facilitates the delocalization the generated charge carriers. To understand how the backbone and side chain structures affect the doping efficiency in these polymers, chemical oxidation experiments were performed sequentially by drop-casting oxidant solution onto as-cast polymer films. After 30 seconds, the films were rinsed and dried prior to measuring their absorption profiles and solid-state conductivity. A doping time of 30 seconds was chosen to ensure that all polymers were fully oxidized (Fig. S10), but short enough so that no film delamination occurred. Tris(4-bromophenyl)ammoniumyl hexachloroantimonate (commonly referred to as Magic Blue, $E_{1/2}$ vs Fc/Fc^+ = 0.70 V)[55] was chosen as the chemical oxidant as it is a strong electron acceptor that can effectively oxidize all polymers and provide a stable $SbCl_6$ anion as a charge compensating dopant ion. Electrochemical doping was carried out in a three-electrode cell in the presence of a $TBAPF_6$ electrolyte salt dissolved in propylene carbonate.

Upon chemical oxidation with Magic Blue, all polymers are converted to their fully oxidized state as we observe full bleaching of the neutral state absorbance (Fig. S10). As we will show later, this is similar to the doping level that is achieved through electrochemical doping. The AFM images taken after doping with Magic Blue (Fig. S11) show that the fibrillar features in the as-cast Ac polymer films disappear, but doping does

not alter either the lamellar or π-π stacking distances in the bulk of the polymer films, as seen in the GIWAXS data in Fig. 2. Furthermore, these GIWAXS images show that this doping process does not alter the directionality of the ordering, as we do not see an alteration of the scattering pattern. For example, for the Ac-EH polymer, we see high scattering intensity in the same region of the scattering image, but the distinct peaks observed in the as cast film (Fig. 1b) are now broader. For the other three polymers we do not see any differences in the shapes of the scattering patterns, but the overall scattering intensity is increased, which can be clearly seen in the linecuts (Fig. S7b). This intensity increase implies that a larger number of polymer chains are intermolecularly aligned after doping, indicating that the overall degree of crystallinity in the polymer film is increased.

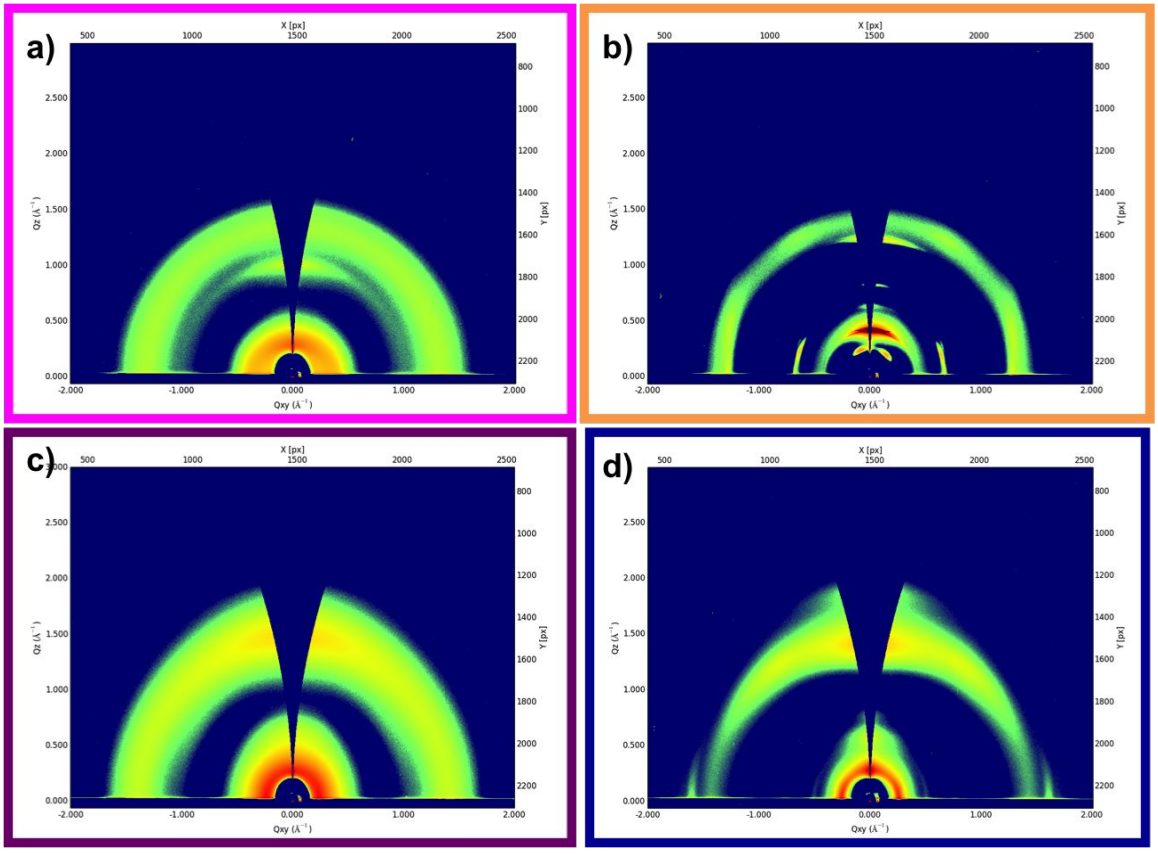

Fig. 2: GIWAXS images of blade-coated polymer films of (a) Pro-EH, (b) Ac-EH, (c) Pro-Oct, (d) Ac-Oct after exposure of the films to a 0.01 M solution of Magic Blue in propylene carbonate for 30 seconds.

After doping with Magic Blue, all polymer films demonstrate an enhancement in their solid-state conductivity, increasing from below 10^{-5} S cm^{-1} in the as cast state up to 10^{0} S cm^{-1} (Fig. S12). For both the Pro and Ac polymers, a significant enhancement in solid-state conductivity is observed when using linear side chains resulting in conductivities on the order of 10^{-1} to 10^{0} S cm^{-1}, whereas the branched side chain analogues which exhibit conductivities on the order of 10^{-3} S cm^{-1}. The values for the polymers with linear side chains are comparable to the linear oligoether functionalized poly(ProDOT), doped with F4TCNQ (0.8 S cm^{-1}).[51] Interestingly, with this family, a larger change in solid-state conductivity is observed when altering the side chain but not the polymer backbone. The higher solid-state conductivity measured for Pro-Oct and Ac-Oct suggest that the linear alkyl chains promote intermolecular interactions that facilitate delocalization of charge carriers both along and across polymer chains. Furthermore, we note that a directionality preference does not affect the observed solid-state conductivity after doping. When comparing the GIWAXS images of Pro-Oct and Ac-Oct (Fig. 2c and 2d), we see that Pro-Oct has no directionality preference relative to the substrate, whereas Ac-Oct as a slight face-on orientation. Previous work has shown that face-on orientations can lead to enhanced charge transfer,[56] however, with this family of polymers we do not observe this as the isotropic Pro-Oct demonstrates the highest solid-state conductivity after doping.

In order to develop a deeper understanding of the impact of structural alteration of side chain and repeat unit on the electrochemical doping process, the polymers were probed by differential pulse voltammetry (DPV) and cyclic voltammetry (CV). Fig. 3a shows the differential pulse voltammograms (Fig. S13) taken of the as-cast polymers in order to discern and compare the polymers' initial propensity to oxidize, which depends on how easily electrons can be extracted from parts of the film that are in close proximity to the underlying electrode as well as a polymer's ionization potential. The onset of oxidation for Pro-EH, Pro-Oct, and Ac-Oct is around 0.1 V, whereas Ac-EH does not begin to oxidize until after 0.3 V. After electrochemical conditioning (Fig. S13), the onset of oxidation of Pro-Oct decreases by ca. 0.2 V indicating that the film undergoes a structural reorganization that extends the effective conjugation length, and as a result, the annealed Pro-Oct becomes easier to oxidize than Ac-Oct. The higher oxidation potential of the Ac polymers is, in part, due to the lack of the propylene bridge, which changes the ability of the lone pair of electrons on the oxygen atoms to interact with the conjugated π-system of the thiophene ring. In addition, the onset of oxidation is affected by steric effects from the side chains where the bulkier EH chains result in higher oxidation potentials for both Pro and Ac polymers (Fig. 3b, 3c and S13). This effect is more drastic for the Ac polymers as the side chains are directly substituted on to the thiophene ring.

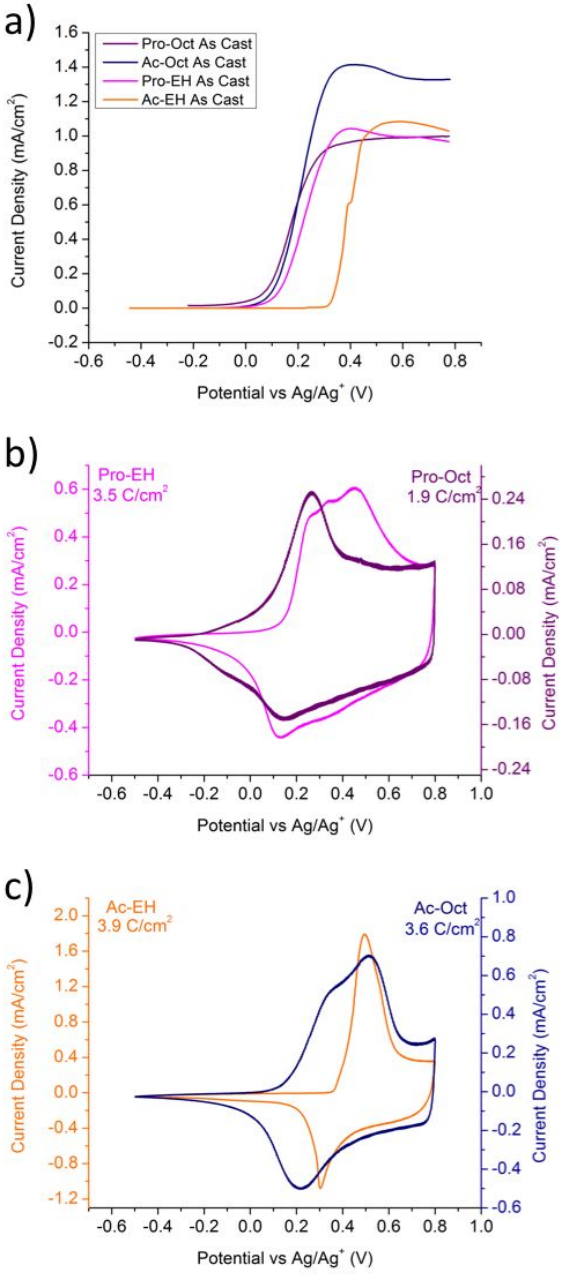

Fig. 3: Differential pulse voltammograms (a) and cyclic voltammograms (b) and (c) of Pro-EH (magenta), Ac-EH (orange), Pro-Oct (purple), and Ac-Oct (navy blue) on a glassy carbon electrode in 0.5 M $TBAPF_6$/PC. Cyclic voltammograms were taken at a scan rate of 50 mV/s.

This different steric effects induced by the side chains is supported by the neutral state optical spectra (green absorbance curves in Fig. 4) where the λ_{max} of Ac-EH is 495

nm, i.e. 55 nm more blue-shifted compared to Ac-Oct with a λ_{max} at 550 nm. In contrast, the Pro polymers show no pronounced spectral difference despite the large difference in their onsets of oxidation, suggesting that steric interactions from the side chains are not the main reason for the observed difference in the onset of oxidation. This is likely due to the fact that the side chains in the Pro polymers are not directly attached to the conjugated backbone, but rather through a neopentyl-type linkage within the 3,4-dioxypropylene bridge. A difference in the onset of oxidation between polymers with linear and branched side chains has also been made in poly(phenylene)-based materials where it was proposed that more bulky ethylhexyloxy side chains can act as insulating barriers between the polymer film and electrode and increase the energy barrier for electrochemical oxidation.[57] Here, the Ac polymers demonstrate enhanced ordering and the presence of distinct phases, which seems to contribute to a more difficult conformational change during polymer oxidation. Based on the GIWAXS data (Fig. 1 and 2), the polymers with linear side chains have a more isotropic scattering pattern compared to the branched side chain counterparts, i.e. for this family of polymers disorder appears to be beneficial for electrochemical oxidation.

Due to the optical changes that are induced upon electrochemical doping, we are able to monitor the extent of doping using *in situ* UV-vis-NIR. Fig. 4 shows the absorption profiles of each polymer film as a function of applied potential. The spectra highlighted in red correspond to the onset of oxidation of the electrochemically conditioned films (for Ac-Oct the onset of oxidation corresponds to the curve at 0.2 V in cyan). The potential where the first optical change is observed increases from Pro-Oct (-0.1 V), to Pro-EH (0.1 V), to Ac-Oct (0.2 V), and finally to Ac-EH (0.4 V), which is in excellent agreement with the

cyclic voltammograms in Fig. 3. Comparing all polymers at 0.2 V (cyan curves), we observe that both Pro polymers have reached a higher doping level than the Ac analogues at this potential as evidenced by a significant decrease in their π-π^* absorption peak as well as the appearance of charge carrier bands at ca. 900 nm and above 1200 nm. By 0.6 V the π-π^* peak for both Pro polymers and the Ac-Oct has been fully depleted and there are no significant changes in the NIR indicating that the materials have been fully doped as increasing the potential further does not affect the doping level. For the Ac-EH polymer full bleaching of the π-π^* absorption peak does not occur until 0.7 V. For all polymers, the spectra corresponding to the fully bleached state matches that of the films that were doped with Magic Blue (Fig. S10) demonstrating that both chemical and electrochemical doping routes are effective in converting the polymers from the neutral to their fully doped forms.

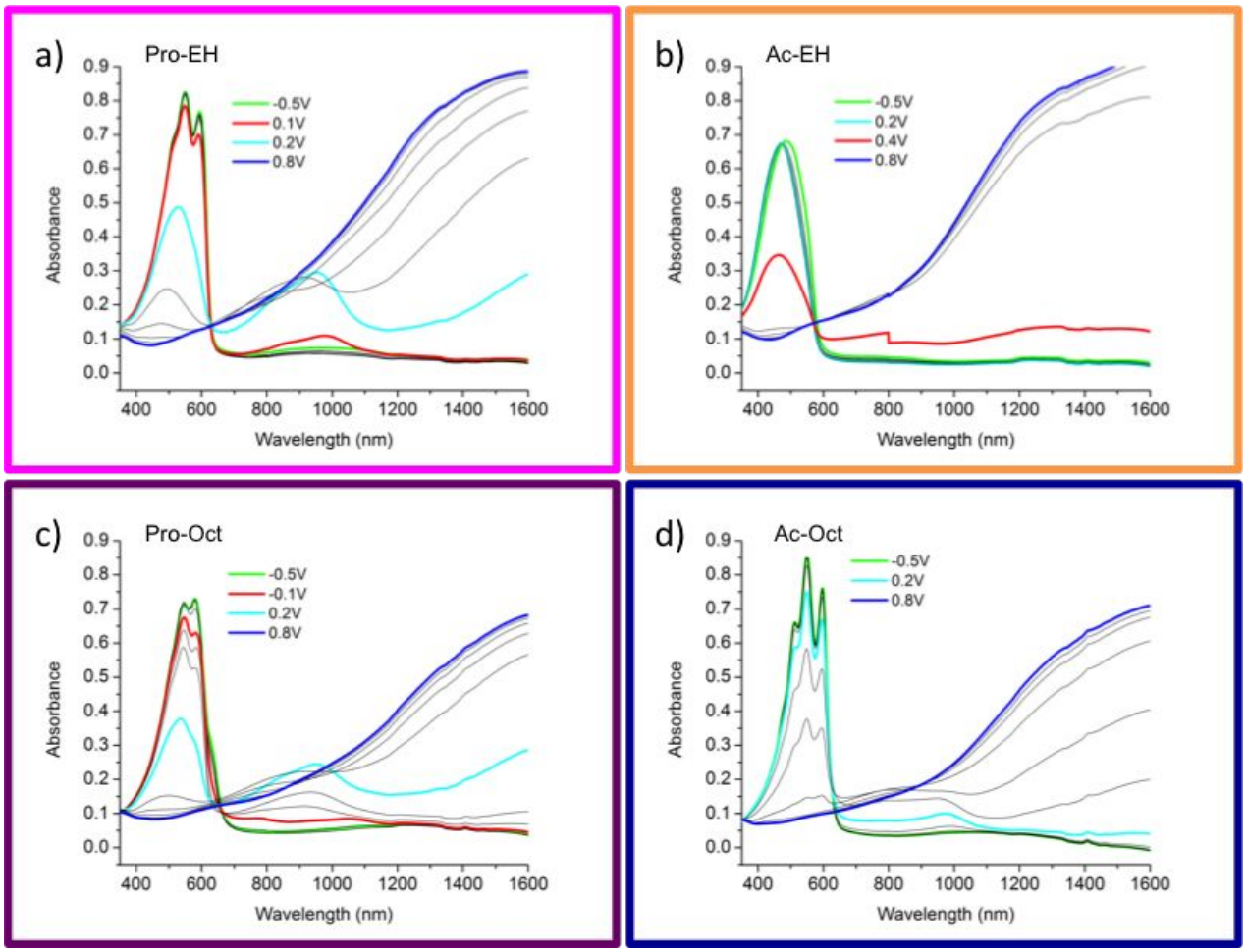

Fig. 4: *In situ* UV-vis absorption spectra as a function of electrochemical doping level (-0.5 V to 0.8 V, 0.1 V increments) for (a) Pro-EH, (b) Ac-EH, (c) Pro-Oct, and (d) Ac-Oct films on ITO/glass in 0.5 M $TBAPF_6$/PC.

To better illustrate how the polymer structure affects the rate of the electrochemical doping, we monitored the absorption at λ_{max} as a function of doping level for each polymer film (Fig. S14). The Pro-EH (1.8 s), Pro-Oct (1.2 s), and Ac-Oct (1.2 s) polymers exhibit similar and rapid doping kinetics where the polymers are fully doped in under 2 s, while the Ac-EH polymer, which is the most ordered, is significantly slower, taking 21 s to reach the fully doped state. The polymers functionalized with linear side chains demonstrate

comparable doping kinetics despite the different backbones and a 0.3 V difference in the onset of oxidation.

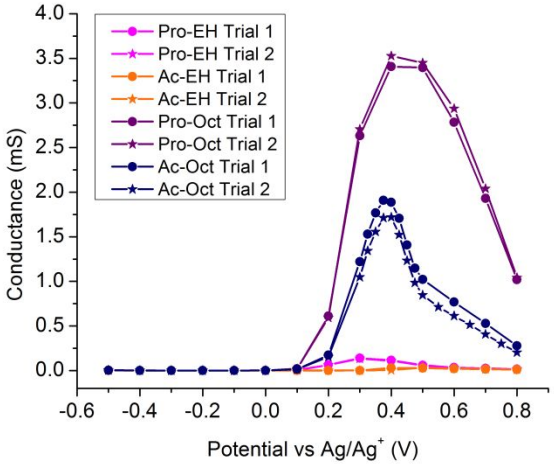

Fig. 5: *In situ* conductance of Pro-EH (magenta), Ac-EH (orange), Pro-Oct (purple), and Ac-Oct (navy blue) on interdigitated electrodes from -0.5 to 0.8 V vs Ag/Ag^+ in 0.5 M $TBAPF_6$/PC.

It is also important to understand how the structure of the polymer repeat unit can affect the electrochemical conductance, as this property could provide some insight as to why we would observe differences in the electrochemical doping kinetics. To experimentally obtain this information, polymer films were drop-cast onto interdigitated microelectrodes and an oxidizing potential was applied to one set of the working electrodes, while at the same time a potential sweep of +/- 5 mV was applied to the other set of the interdigitated electrodes while the current was recorded.[58] Potential sweeps were taken as a function of the applied potential from -0.5 V to 0.8 V vs Ag/Ag^+ with 0.1 V increments as shown in Fig. 5. Reverse direction curves for these experiments (from high to low potential) can be seen in Fig. S15. Maximum conductance values are lower for each polymer on the reverse scan, but are not affected by polymer structure. A turn-on of the

conductance response is observed between 0.1 to 0.2 V for both Pro polymers and for Ac-Oct, whereas the conductance turn-on for Ac-EH does not occur until above 0.4 V. It should be noted that the onset potential of the conductance is higher than the onset of oxidation measured by DPV due to the fundamental differences in the measurements. In DPV, the onset of oxidation measures electron transfer occurring close to the polymer/electrode interface and does not depend upon any long-range charge transport, where the *in situ* conductance measurement requires the charge carriers to transverse across the insulating gap of the interdigitated electrodes. As can be seen in the spectroelectrochemical results in Fig. 4, all polymers except for Ac-EH show a decrease in the π-π* absorption by 0.2 V where we also observe the onset of conductance, indicating Pro-EH, Pro-Oct, and Ac-Oct have all been sufficiently electrochemically doped in order to transport charge carriers across the insulating gap of the interdigitated electrode. While Pro-EH and Pro-Oct have similar doping kinetics (Fig. S14), and have reached a similar doping level at 0.2 V (as evidenced by the absorption curve showing polaron generation and a similar degree of bleaching of the π-π* absorption band, Fig. 4), Pro-Oct has a significantly higher electrochemical conductance. Integrating the CV currents allows us to extract the amount of charge required to complete a redox switch. As seen in Fig. 3, the charge capacity of Pro-EH is 3.5 C/cm^2 and for Pro-Oct it is 1.9 C/cm^2. This implies that a larger number of charge carriers are required to dope the polymer with branched side chains to the achieve the same optical change as the linear side chain analogue. While Ac-Oct only demonstrates a small change in its optical properties at 0.2 V, this relatively low doping level is sufficient charge transport across the gap. Turning to Ac-EH, we do not observe an electrochemical conductance response until 0.4 V, which is in excellent agreement with the spectra in Fig.

4b. For both the Pro and Ac structures, we observe higher electrochemical conductance for polymers substituted with linear side chains. The maximum conductance values are reached at 0.4 V for both Pro-Oct and Ac-Oct. According to Fig. 4, the maximum conductance for Ac-Oct is achieved at a lower doping level than for Pro-Oct as evidenced by the π-π* absorption peak which is fully depleted in Pro-Oct but clearly visible for Ac-Oct. All polymers exhibit a drop in electrochemical conductance at high potential values, above 0.5 V. One interpretation for the conductance drop at higher doping levels is that the polymers reach a maximum number of generated charge carriers, which induces a decrease in charge carrier mobility.

Electrochemical Impedance Spectroscopy

Using the same GC button electrodes as were used for DPV and CV characterization, in situ electrochemical impedance spectroscopy was performed. To study the doping process and the capacitive behavior of the formed charge carriers, electrochemical impedance spectra were recorded as a function of doping level as seen in the Nyquist plot in Fig. 6a. At potentials where the polymer is doped, the charge accumulation process is fitted using a model that includes the electrolyte resistance $R_{el,}$ a Warburg element R_w that relates the charging rate within the polymer film to ion transport, and a low frequency (0.1 – 1 Hz) independent pseudocapacitance CPE_ϕ (dQ/dV).[59-61] To compensate for heterogeneous charge carriers distribution in the polymer films and to improve the fitting quality, the capacitance is fitted using a CPE generic transfer function described by

$$Z_{\mathrm{CPE}} = \left[Y_0\,(j\omega)^n\right]^{-1} \quad (1)$$

where Y_0 is the numerical value of the admittance at ω =1 rad s^{-1}, $\omega = 2\pi f$ is the angular frequency in rad s^{-1} and $0.8 < n < 1$ is the CPE exponent used as a gauge for surface roughness.

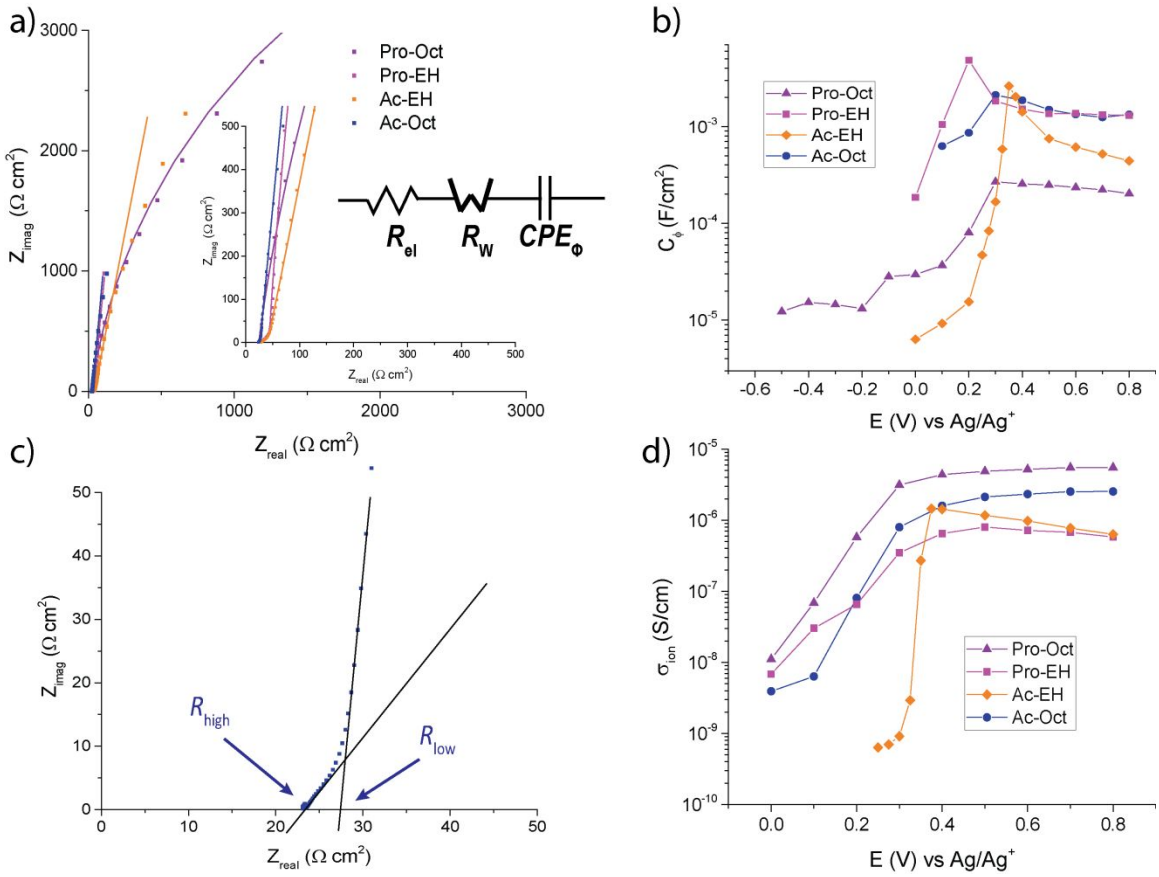

Fig. 6: (a) The experimental (data points) and fitted (line) electrochemical impedance data of the oxidized Pro-EH (magenta), Ac-EH (orange), Pro-Oct (purple), and Ac-Oct (navy blue) on a polished glassy carbon electrode at 0.8 V vs Ag/Ag^+ in $TBAPF_6$/PC with the electric equivalent circuit to fit the mid and low frequency data. (b) The fitted pseudocapacitance (C_Φ) extracted from the EIS data as a function of applied potential. (c) The extraction procedure for the ionic conductivity using the impedance spectrum of Ac-Oct measured at 0.8 V. (d) The extracted ionic conductivities of all polymers from 0.0 to 0.8V vs Ag/Ag^+ in $TBAPF_6$/PC.

The fitted parameters give us valuable information about the number of charge carriers in the polymer as a function of the doping level. The pseudocapacitance is related to charge carrier accumulation that is linearly proportional to the applied potential, which for CPs means that the charge carriers that contribute to a pseudocapacitance are in redox-active sites of comparable energy resulting in fast charge transfer along, across, and/or between chains. The potential dependence of the pseudocapacitance for these polymers (Fig. 6b) matches the current registered in the cyclic voltammograms (Fig. 3), but not the potential dependence of the *in situ* conductance results in Fig. 6. As shown in Fig. 6b, the pseudocapacitance of Pro-Oct at high doping levels is lower than that of the other polymers, which is in good agreement with the trend in charge capacity determined by CV. Both polymers with EH side chains have a high pseudocapacitance while the conductance is negligible.

When focusing on the ionic transport process in the oxidized polymer films, we use a finite transmission line model as described by Pickup et al.[62] As illustrated in Fig. 6c, this model predicts that the high-frequency intercept with the real axis (R_{high}) gives us the electrolyte resistance, R_{el}, and that the intercept of the extrapolation of the low-frequency linear portion with the real axis translates to $R_{el} + (R_{ion}/3) = (R_{low})$ assuming ion transport, rather than electron transport, is the rate limiting process. In Fig. 6d, the ionic conductivity is calculated using

$$\sigma_{ion} = \frac{t}{3(R_{low} - R_{high})A} \quad (2)$$

where t is the polymer film thickness (with an average of 300 nm) and A is the electrode area. The ionic conductivity profiles in Fig. 6d demonstrate that the linear side chain polymers have a higher ionic conductivity at high doping levels (between 0.5 to 0.8 V) than the the EH polymers. These results show that when incorporating linear side chains in these disubstituted dioxythiophene polymers, the CP has a higher electrochemical conductance and that ions can more easily diffuse into the swollen polymer film at high potentials. Notice that a higher pseudocapacitance and ionic conductivity does not necessarily correlate with a high measured film conductance.

Discussion:

Given the full analysis presented in this study, a "one size fits all" structure-property relationship is not immediately evident from the observed results. A combination of both electrochemical and surface analysis techniques broadens our perspective and gives us a better understanding of the mixed transport processes in the polymer film.

In this work it was shown that, incorporating linear side chains onto dioxythiophene homopolymers result in an increase of the *in situ* conductance and solid-state conductivity compared their branched counterparts. Comparing Pro-Oct and Ac-Oct, we see that Pro-Oct has a lower onset of oxidation than Ac-Oct, despite both have similar optical gaps in the neutral state suggesting similar degrees of torsion along the backbone in the neutral state. According to the GIWAXS data, Ac-Oct demonstrates a higher degree of ordering in both the neutral and doped state, and an as-cast fibril-like topology according to the AFM measurements. Ac-Oct shows a lower *in situ* conductance and solid-state conductivity compared to Pro-Oct, however in terms of electrochemical doping, this polymer is doped to a lesser degree at the same potential. Collectively, the charge transport and

morphological characterizations results indicate that the charge transport properties of Ac-Oct are affected by its more ordered morphology, which results in a material that is more difficult to oxidize and that has lower electrochemical and solid-state conductivity. While the enhanced order in the Ac-Oct polymer helps to generate more charge carriers compared to Pro-Oct, based on the both the charge capacity and the pseudocapacitance measured by EIS, these extra charge carriers are not able to transverse the bulk of the film as effectively. We see that while order is important to ensure charge transport between chains, too much ordering and a lack of connection between ordered domains can result in materials that do not easily oxidize even if the backbone of the polymer is relatively planar. The fact that Pro-Oct shows consistently the highest electrochemical conductance, and solid-state conductivity means that isotropic and more homogenous ordering and a smooth morphology are preferred in these polymer systems making them easier to electrochemically oxidize, and for facilitating faster transport of both charge carriers and dopant ions.

Turning to the branched side chain polymers, Pro-EH shows faster doping kinetics than its Ac analogue. The Ac-EH has the lowest electrochemical conductance, and solid-state conductivity in combination with high degrees of anisotropic polymer ordering (with very specific scattering angles) and a fibril-like topography. These results imply that tighter packing of polymer chains in the film inhibit oxidation and redox switching. Furthermore, the torsional strain in the backbone causes conformational twisting making the film harder to oxidize than the more amorphous Pro materials. In comparison to polymers with the Oct side chains, Pro-EH demonstrates low electrochemical conductance and solid-state conductivity. This polymer is also highly amorphous, with little to no order demonstrated

by both GIWAXS and AFM images. Its relaxed backbone geometry explains why Pro-EH is easy to oxidize, but its amorphous nature is what inhibits charges from effectively moving from one chain to another through the film. The bulkier EH side chains slow down ionic transport and explain the loss of strong intermolecular interactions like π-π stacks between the polymer chains resulting in an overall low conductivity.

Conclusions:

This study aims to help in understanding the delicate balance of material properties that is required to design new state-of-the-art materials for a wide range of applications. Studying this family of polymers demonstrates that a slight alteration in the polymer repeat unit structure results in large effects on the polymer's charge transport properties. Moreover, we demonstrated that incorporating linear side chains as compared to branched side chains enhances electrochemical as well as solid-state charge transport in both Pro and Ac polymers. Here, it is shown that intermolecular order of polymer chains plays an important role in the materials' ability to transport charges, with the understanding that some degree of order enhances charge hopping between the chains and that too much order induces separation between ordered and disordered domains, which inhibits the ease of oxidation. Polymers that demonstrated high electrochemical conductance also demonstrated high solid-state conductivity, indicating that the ideas presented in this work are applicable for both types of charge transport and their corresponding applications.

Author Contributions:

M.A.O. synthesized and confirmed the structure of the polymers Ac-EH and Ac-Oct. J.F.P. synthesized and confirmed the structure of Pro-Oct. M.D.K. carried out and analyzed EIS

experiments. S.P. carried the planning, execution, and evaluation of all other experimentation corresponding to the redox and solid-state measurements. A.M. Ö. assisted with the analysis of the collected data. All authors contributed to writing this manuscript and have given approval of the final version.

Funding:
The following funding sources (ONR grant numbers: N00014-16-1-2165 and N00014-18-1-2222) have been used in order to generate this work.

Notes:
The authors declare the following competing financial interest (s): Electrochromic polymer technology developed at the University of Florida and the Georgia Institute of Technology has been licensed to NXN Licensing. J.R.R. and A.M.Ö. serves as a consultant to NXN Licensing.

Acknowledgements:
The authors would like to gratefully acknowledge Maged Abdelsami in the group of Dr. Michael Toney at Stanford for assistance with the GIWAXS data interpretation. In addition, thank you to D. Eric Shen for advice and assistance with data analysis discussion and interpretation. Finally, we would like to thank Graham Collier for performing Gel Permeation Chromatography experiments to measure molecular weights and distributions of the polymers in this study.

References:

(1) Jacobs, I. E.; Aasen, E. W.; Oliveira, J. L.; Fonseca, T. N.; Roehling, J. D.; Li, J.; Zhang, G.; Augustine, M. P.; Mascal, M.; Moulé, A. J. Comparison of solution-mixed

and sequentially processed P3HT:F4TCNQ films: effect of doping-induced aggregation on film morphology. *Journal of Materials Chemistry C* **2016**, *4*, 3454-3466.

(2) Jacobs, I. E.; Moulé, A. J. Controlling Molecular Doping in Organic Semiconductors. *Advanced Materials* **2017**, *29*, 1703063.

(3) Bubnova, O.; Khan, Z. U.; Malti, A.; Braun, S.; Fahlman, M.; Berggren, M.; Crispin, X. Optimization of the thermoelectric figure of merit in the conducting polymer poly(3,4-ethylenedioxythiophene). *Nat Mater* **2011**, *10*, 429-433.

(4) Scholes, D. T.; Yee, P. Y.; Lindemuth, J. R.; Kang, H.; Onorato, J.; Ghosh, R.; Luscombe, C. K.; Spano, F. C.; Tolbert, S. H.; Schwartz, B. J. The Effects of Crystallinity on Charge Transport and the Structure of Sequentially Processed F4TCNQ-Doped Conjugated Polymer Films. *Advanced Functional Materials* **2017**, *27*, 1702654.

(5) Chiang, C. K.; Gau, S. C.; Fincher, C. R.; Park, Y. W.; MacDiarmid, A. G.; Heeger, A. J. Polyacetylene, (CH)x: n‐type and p‐type doping and compensation. *Applied Physics Letters* **1978**, *33*, 18-20.

(6) Schottland, P.; Zong, K.; Gaupp, C. L.; Thompson, B. C.; Thomas, C. A.; Giurgiu, I.; Hickman, R.; Abboud, K. A.; Reynolds, J. R. Poly(3,4-alkylenedioxypyrrole)s: Highly Stable Electronically Conducting and Electrochromic Polymers. *Macromolecules* **2000**, *33*, 7051-7061.

(7) Sonmez, G.; Schottland, P.; Zong, K.; Reynolds, J. R. Highly transmissive and conductive poly[(3,4-alkylenedioxy)pyrrole-2,5-diyl] (PXDOP) films prepared by air or transition metal catalyzed chemical oxidation. *Journal of Materials Chemistry* **2001**, *11*, 289-294.

(8) Higgins, A.; Mohapatra, S. K.; Barlow, S.; Marder, S. R.; Kahn, A. Dopant controlled trap-filling and conductivity enhancement in an electron-transport polymer. *Applied Physics Letters* **2015**, *106*, 163301.

(9) Pittelli, S. L.; Shen, D. E.; Österholm, A. M.; Reynolds, J. R. Chemical Oxidation of Polymer Electrodes for Redox Active Devices: Stabilization through Interfacial Interactions. *ACS Applied Materials & Interfaces* **2018**, *10*, 970-978.

(10) Schroeder, A. H.; Kaufman, F. B. The influence of polymer morphology on polymer film electrochemistry. *Journal of Electroanalytical Chemistry and Interfacial Electrochemistry* **1980**, *113*, 209-224.

(11) Groenendaal, L.; Zotti, G.; Aubert, P.-H.; Waybright, S. M.; Reynolds, J. R. Electrochemistry of Poly(3,4-alkylenedioxythiophene) Derivatives. *Advanced Materials* **2003**, *15*, 855-879.

(12) Holliday, S.; Donaghey, J. E.; McCulloch, I. Advances in Charge Carrier Mobilities of Semiconducting Polymers Used in Organic Transistors. *Chemistry of Materials* **2014**, *26*, 647-663.

(13) Holliday, S.; Li, Y.; Luscombe, C. K. Recent advances in high performance donor-acceptor polymers for organic photovoltaics. *Progress in Polymer Science* **2017**, *70*, 34-51.

(14) Endrődi, B.; Mellár, J.; Gingl, Z.; Visy, C.; Janáky, C. Molecular and Supramolecular Parameters Dictating the Thermoelectric Performance of Conducting Polymers: A Case Study Using Poly(3-alkylthiophene)s. *The Journal of Physical Chemistry C* **2015**, *119*, 8472-8479.

(15) Bubnova, O.; Khan, Z. U.; Malti, A.; Braun, S.; Fahlman, M.; Berggren, M.; Crispin, X. Optimization of the thermoelectric figure of merit in the conducting polymer poly(3,4-ethylenedioxythiophene). *Nat Mater* **2011**, *10*, 429-433.

(16) Kim, Y. H.; Sachse, C.; Machala, M. L.; May, C.; Müller-Meskamp, L.; Leo, K. Highly Conductive PEDOT:PSS Electrode with Optimized Solvent and Thermal Post-Treatment for ITO-Free Organic Solar Cells. *Advanced Functional Materials* **2011**, *21*, 1076-1081.

(17) Kim, N.; Kee, S.; Lee, S. H.; Lee, B. H.; Kahng, Y. H.; Jo, Y.-R.; Kim, B.-J.; Lee, K. Highly Conductive PEDOT:PSS Nanofibrils Induced by Solution-Processed Crystallization. *Advanced Materials* **2014**, *26*, 2268-2272.

(18) Argun, A. A.; Cirpan, A.; Reynolds, J. R. The First Truly All-Polymer Electrochromic Devices. *Advanced Materials* **2003**, *15*, 1338-1341.

(19) Otley, M. T.; Alamer, F. A.; Zhu, Y.; Singhaviranon, A.; Zhang, X.; Li, M.; Kumar, A.; Sotzing, G. A. Acrylated Poly(3,4-propylenedioxythiophene) for Enhancement of Lifetime and Optical Properties for Single-Layer Electrochromic Devices. *ACS Applied Materials & Interfaces* **2014**, *6*, 1734-1739.

(20) Jensen, J.; Hösel, M.; Kim, I.; Yu, J.-S.; Jo, J.; Krebs, F. C. Fast Switching ITO Free Electrochromic Devices. *Advanced Functional Materials* **2014**, *24*, 1228-1233.

(21) Cai, G.; Wang, J.; Lee, P. S. Next-Generation Multifunctional Electrochromic Devices. *Accounts of Chemical Research* **2016**, *49*, 1469-1476.

(22) Dubal, D. P.; Ayyad, O.; Ruiz, V.; Gomez-Romero, P. Hybrid energy storage: the merging of battery and supercapacitor chemistries. *Chemical Society Reviews* **2015**, *44*, 1777-1790.

(23) Bryan, A. M.; Santino, L. M.; Lu, Y.; Acharya, S.; D'Arcy, J. M. Conducting Polymers for Pseudocapacitive Energy Storage. *Chemistry of Materials* **2016**, *28*, 5989-5998.

(24) Snook, G. A.; Kao, P.; Best, A. S. Conducting-polymer-based supercapacitor devices and electrodes. *Journal of Power Sources* **2011**, *196*, 1-12.

(25) Pabst, O.; Perelaer, J.; Beckert, E.; Schubert, U. S.; Eberhardt, R.; Tünnermann, A. All inkjet-printed piezoelectric polymer actuators: Characterization and applications for micropumps in lab-on-a-chip systems. *Organic Electronics* **2013**, *14*, 3423-3429.

(26) Okuzaki, H.; Kuwabara, T.; Funasaka, K.; Saido, T. Humidity-Sensitive Polypyrrole Films for Electro-Active Polymer Actuators. *Advanced Functional Materials* **2013**, *23*, 4400-4407.

(27) Otero, T. F.; Martinez, J. G.; Arias-Pardilla, J. Biomimetic electrochemistry from conducting polymers. A review: Artificial muscles, smart membranes, smart drug delivery and computer/neuron interfaces. *Electrochimica Acta* **2012**, *84*, 112-128.

(28) Smela, E. Conjugated Polymer Actuators for Biomedical Applications. *Advanced Materials* **2003**, *15*, 481-494.

(29) Nielsen, C. B.; Giovannitti, A.; Sbircea, D.-T.; Bandiello, E.; Niazi, M. R.; Hanifi, D. A.; Sessolo, M.; Amassian, A.; Malliaras, G. G.; Rivnay, J.; McCulloch, I. Molecular Design of Semiconducting Polymers for High-Performance Organic Electrochemical Transistors. *Journal of the American Chemical Society* **2016**, *138*, 10252-10259.

(30) Simon, D. T.; Gabrielsson, E. O.; Tybrandt, K.; Berggren, M. Organic Bioelectronics: Bridging the Signaling Gap between Biology and Technology. *Chemical Reviews* **2016**, *116*, 13009-13041.

(31) Rivnay, J.; Owens, R. M.; Malliaras, G. G. The Rise of Organic Bioelectronics. *Chemistry of Materials* **2014**, *26*, 679-685.

(32) Mei, J.; Bao, Z. Side Chain Engineering in Solution-Processable Conjugated Polymers. *Chemistry of Materials* **2014**, *26*, 604-615.

(33) Kim, M. J.; Jung, A. R.; Lee, M.; Kim, D.; Ro, S.; Jin, S.-M.; Nguyen, H. D.; Yang, J.; Lee, K.-K.; Lee, E.; Kang, M. S.; Kim, H.; Choi, J.-H.; Kim, B.; Cho, J. H. Structure–Property Relationships of Semiconducting Polymers for Flexible and Durable Polymer Field-Effect Transistors. *ACS Applied Materials & Interfaces* **2017**, *9*, 40503-40515.

(34) Yim, K.-H.; Whiting, G. L.; Murphy, C. E.; Halls, J. J. M.; Burroughes, J. H.; Friend, R. H.; Kim, J.-S. Controlling Electrical Properties of Conjugated Polymers via a Solution-Based p-Type Doping. *Advanced Materials* **2008**, *20*, 3319-3324.

(35) Kuei, B.; Gomez, E. D. Chain conformations and phase behavior of conjugated polymers. *Soft Matter* **2017**, *13*, 49-67.

(36) Hildner, R.; Köhler, A.; Müller-Buschbaum, P.; Panzer, F.; Thelakkat, M. π-Conjugated Donor Polymers: Structure Formation and Morphology in Solution, Bulk and Photovoltaic Blends. *Advanced Energy Materials* **2017**, *7*, 1700314.

(37) Richter, L. J.; DeLongchamp, D. M.; Amassian, A. Morphology Development in Solution-Processed Functional Organic Blend Films: An In Situ Viewpoint. *Chemical Reviews* **2017**, *117*, 6332-6366.

(38) Yang, X.; Loos, J. Toward High-Performance Polymer Solar Cells: The Importance of Morphology Control. *Macromolecules* **2007**, *40*, 1353-1362.

(39) Heinze, J.; Frontana-Uribe, B. A.; Ludwigs, S. Electrochemistry of Conducting Polymers—Persistent Models and New Concepts. *Chemical Reviews* **2010**, *110*, 4724-4771.

(40) Dietrich, M.; Heinze, J.; Heywang, G.; Jonas, F. Electrochemical and spectroscopic characterization of polyalkylenedioxythiophenes. *Journal of Electroanalytical Chemistry* **1994**, *369*, 87-92.

(41) Zou, Y.; Najari, A.; Berrouard, P.; Beaupré, S.; Réda Aïch, B.; Tao, Y.; Leclerc, M. A Thieno[3,4-c]pyrrole-4,6-dione-Based Copolymer for Efficient Solar Cells. *Journal of the American Chemical Society* **2010**, *132*, 5330-5331.

(42) Piliego, C.; Holcombe, T. W.; Douglas, J. D.; Woo, C. H.; Beaujuge, P. M.; Fréchet, J. M. J. Synthetic Control of Structural Order in N-Alkylthieno[3,4-c]pyrrole-4,6-dione-Based Polymers for Efficient Solar Cells. *Journal of the American Chemical Society* **2010**, *132*, 7595-7597.

(43) Himmelberger, S.; Duong, D. T.; Northrup, J. E.; Rivnay, J.; Koch, F. P. V.; Beckingham, B. S.; Stingelin, N.; Segalman, R. A.; Mannsfeld, S. C. B.; Salleo, A. Role of Side-Chain Branching on Thin-Film Structure and Electronic Properties of Polythiophenes. *Advanced Functional Materials* **2015**, *25*, 2616-2624.

(44) Kang, I.; Yun, H.-J.; Chung, D. S.; Kwon, S.-K.; Kim, Y.-H. Record High Hole Mobility in Polymer Semiconductors via Side-Chain Engineering. *Journal of the American Chemical Society* **2013**, *135*, 14896-14899.

(45) McDearmon, B.; Page, Z. A.; Chabinyc, M. L.; Hawker, C. J. Organic electronics by design: the power of minor atomic and structural changes. *Journal of Materials Chemistry C* **2018**, *6*, 3564-3572.

(46) Giovannitti, A.; Sbircea, D.-T.; Inal, S.; Nielsen, C. B.; Bandiello, E.; Hanifi, D. A.; Sessolo, M.; Malliaras, G. G.; McCulloch, I.; Rivnay, J. Controlling the mode of operation of organic transistors through side-chain engineering. *Proceedings of the National Academy of Sciences* **2016**, *113*, 12017-12022.

(47) Dong, B. X.; Nowak, C.; Onorato, J. W.; Strzalka, J.; Escobedo, F. A.; Luscombe, C. K.; Nealey, P. F.; Patel, S. N. Influence of Side-Chain Chemistry on Structure and Ionic Conduction Characteristics of Polythiophene Derivatives: A Computational and Experimental Study. *Chemistry of Materials* **2019**, *31*, 1418-1429.

(48) Flagg, L. Q.; Bischak, C. G.; Onorato, J. W.; Rashid, R. B.; Luscombe, C. K.; Ginger, D. S. Polymer Crystallinity Controls Water Uptake in Glycol Side-Chain Polymer Organic Electrochemical Transistors. *Journal of the American Chemical Society* **2019**, *141*, 4345-4354.

(49) Cirpan, A.; Argun, A. A.; Grenier, C. R. G.; Reeves, B. D.; Reynolds, J. R. Electrochromic devices based on soluble and processable dioxythiophene polymers. *Journal of Materials Chemistry* **2003**, *13*, 2422-2428.

(50) Ponder Jr., J. F.; Menon, A. K.; Dasari, R. R.; Pittelli, S. L.; Thorley, K. J.; Yee, S. K.; Marder, S. R.; Reynolds, J. R. Conductive, Solution-Processed Dioxythiophene Copolymers for Thermoelectric and Transparent Electrode Applications. *Advanced Energy Materials*, *0*, 1900395.

(51) Mazaheripour, A.; Thomas, E. M.; Segalman, R. A.; Chabinyc, M. L. Nonaggregating Doped Polymers Based on Poly(3,4-Propylenedioxythiophene). *Macromolecules* **2019**, *52*, 2203-2213.

(52) Padilla, J.; Österholm, A. M.; Dyer, A. L.; Reynolds, J. R. Process controlled performance for soluble electrochromic polymers. *Solar Energy Materials and Solar Cells* **2015**, *140*, 54-60.

(53) Dyer, A. L.; Craig, M. R.; Babiarz, J. E.; Kiyak, K.; Reynolds, J. R. Orange and Red to Transmissive Electrochromic Polymers Based on Electron-Rich Dioxythiophenes. *Macromolecules* **2010**, *43*, 4460-4467.

(54) Duong, D. T.; Wang, C.; Antono, E.; Toney, M. F.; Salleo, A. The chemical and structural origin of efficient p-type doping in P3HT. *Organic Electronics* **2013**, *14*, 1330-1336.

(55) Connelly, N. G.; Geiger, W. E. Chemical Redox Agents for Organometallic Chemistry. *Chemical Reviews* **1996**, *96*, 877-910.

(56) Rathgeber, S.; Perlich, J.; Kühnlenz, F.; Türk, S.; Egbe, D. A. M.; Hoppe, H.; Gehrke, R. Correlation between polymer architecture, mesoscale structure and photovoltaic performance in side-chain-modified poly(p-arylene-ethynylene)-alt-poly(p-arylene-vinylene): PCBM bulk-heterojunction solar cells. *Polymer* **2011**, *52*, 3819-3826.

(57) Egbe, D. A. M.; Nguyen, L. H.; Hoppe, H.; Mühlbacher, D.; Sariciftci, N. S. Side Chain Influence on Electrochemical and Photovoltaic Properties of Yne-Containing Poly(phenylene vinylene)s. *Macromolecular Rapid Communications* **2005**, *26*, 1389-1394.

(58) Imae, I.; Mashima, T.; Sagawa, H.; Komaguchi, K.; Ooyama, Y.; Harima, Y. In situ conductivity measurements of polythiophene partially containing 3,4-ethylenedioxythiophene and 3-hexylthiophene. *Journal of Solid State Electrochemistry* **2015**, *19*, 71-76.

(59) Musiani, M. M. Characterization of electroactive polymer layers by electrochemical impedance spectroscopy (EIS). *Electrochimica Acta* **1990**, *35*, 1665-1670.

(60) Amemiya, T. H., K.; Fujishima, A. Faradaic Charge Transfer with Double-Layer Charging and/or Adsorption-Related Charging at Polymer-Modified Electrodes As Observed by Color Impedance Spectroscopy. *J. Phys. Chem.* **1993**, *97*, 9736-9740.

(61) Ogihara, N.; Itou, Y.; Sasaki, T.; Takeuchi, Y. Impedance Spectroscopy Characterization of Porous Electrodes under Different Electrode Thickness Using a Symmetric Cell for High-Performance Lithium-Ion Batteries. *The Journal of Physical Chemistry C* **2015**, *119*, 4612-4619.

(62) Pickup, P. G. Alternating current impedance study of a polypyrrole-based anion-exchange polymer. *Journal of the Chemical Society, Faraday Transactions* **1990**, *86*, 3631-3636.

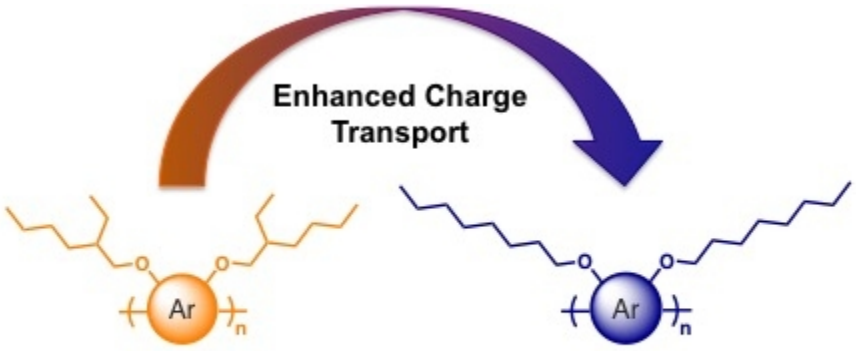

Dioxythiophene polymers incorporating **linear** side chains show higher solid-state conductivity and enhanced redox properties.

157x78mm (72 x 72 DPI)